

We are IntechOpen, the world's leading publisher of Open Access books Built by scientists, for scientists

6,900

Open access books available

186,000

International authors and editors

200M

Downloads

Our authors are among the

154

Countries delivered to

TOP 1%

most cited scientists

12.2%

Contributors from top 500 universities



WEB OF SCIENCE™

Selection of our books indexed in the Book Citation Index
in Web of Science™ Core Collection (BKCI)

Interested in publishing with us?
Contact book.department@intechopen.com

Numbers displayed above are based on latest data collected.
For more information visit www.intechopen.com



Optical Absorption, Charge Separation and Recombination Dynamics in Pb and Sn/Pb Cocktail Perovskite Solar Cells and Their Relationships to the Photovoltaic Properties

Shen Qing, Ogomi Yuhei, Toyoda Taro, Yoshino Kenji and Hayase Shuzi

Additional information is available at the end of the chapter

<http://dx.doi.org/10.5772/62101>

Abstract

Due to the unique characteristics such as simple low-temperature preparation method and high efficiency with a record of over 20%, organometal trihalide perovskite ($\text{CH}_3\text{NH}_3\text{PbI}_3$)-based solid-state hybrid solar cells have attracted an increasing interest since 2012 when it was reported. During the last several years, some of the fundamental photophysical properties of perovskite related to the high photovoltaic performance have been investigated. Optical absorption, charge separation and recombination are very important factors influencing the perovskite solar cell performance. In this chapter, our recent results of optical absorption, charge separation (electron and hole injection) and charge recombination dynamics at each interface in perovskite solar cells, and their relationships to photovoltaic properties will be introduced. Our results suggest that charge recombination is a key factor in improving the performance of the perovskite solar cells.

Keywords: Urbach energy, charge separation, charge recombination, optical absorption, Sn/Pb cocktail perovskite, perovskite

1. Introduction

Organolead halide perovskites in the format of AMX_3 (A=organic molecule, e.g., $\text{CH}_3\text{NH}_3(\text{MA})$, B=Pb, X=Cl, Br, and I) can be easily crystallized from solution at relatively low temperature (i.e., $\leq 100^\circ\text{C}$), which makes it possible to use them as light absorbing materials in different kinds of solar cells. Following the recently reported certified high power conversion efficiency (PCE) of over 20%, [1-12] the interest in organolead halide perovskite-based

organic-inorganic hybrid solid-state solar cells has increased dramatically over the past several years. The higher PCEs of organolead halide perovskites (especially MAPbI₃) result from their unique properties that are key for achieving high photovoltaic performance, which are (1) a direct band gap and a high optical absorption coefficient; [13, 14] (2) large dielectric coefficient leading to smaller exciton binding energy; [15] (3) long photoexcited carrier lifetimes (>100 ns) and long diffusion lengths (100 – 1000 nm or even longer); [16, 17] (4) no deep state defects and very small Urbach energy. [18]

It is reasonable to expect that further improvements in photovoltaic performance can be achieved by increasing the light harvesting up to NIR wavelengths of 1000 nm, since MAPbI₃ perovskite only absorbs light at wavelengths below 800 nm constrained by its optical band gap of 1.5 eV. In addition, practically, Pb-free organometal halide perovskites are preferred due to the potential toxicology issue of Pb. Replacing Pb with Sn or mixing Pb and Sn in organometal halide perovskites can result in increased light harvesting in the NIR region up to 1000 nm [19, 20] and, at the same time, reduce the toxicity issue related to Pb. Several research groups have reported, very recently, Sn-based or Pb/Sn cocktail MASn_xPb_{1-x}I₃ (0 ≤ x ≤ 1) perovskite solar cells. [21-24] However, it is found that the PCE of Sn/Pb cocktail MASn_xPb_{1-x}I₃ perovskite solar cells is far inferior to that of MAPbI₃ perovskite solar cells.

In order to improve the photovoltaic performance of Pb and Sn/Pb cocktail perovskite solar cells, it is critical to gain a thorough understanding of the optical absorption properties, the photoexcited carrier lifetimes, as well as the charge separation and recombination dynamics at each interface. In this chapter, we will focus on recent studies of the optical absorption, photoexcited carrier lifetime, the charge separation and charge recombination dynamics at each interface in perovskite solar cells, including Pb-based and Sn/Pb cocktail perovskite solar cells. The relationships of each of these physical properties to the photovoltaic performance of the solar cells will be discussed and the methodologies for improving the photovoltaic performance of perovskite solar cells will be proposed.

2. Experimental

2.1. Sample preparation

Samples of Pb-based perovskite hybrid solar cells were prepared by the following method. [25] F-doped SnO₂ layered glass (FTO glass, Nippon Sheet Glass Co. Ltd) was patterned using Zn powder and 6 N HCl aqueous solution. Titanium diisopropoxide bis(acetylacetonate) solution in ethanol was sprayed onto this patterned FTO glass at 300 °C to prepare compact TiO₂ layers. Porous TiO₂ layers were fabricated by spin-coating TiO₂ pastes of different nanoparticle sizes (18 nm: PST-18NR or 30 nm: PST-30NRD, JGC Catalysts and Chemicals Ltd.) in ethanol (TiO₂ paste : ethanol = 1:2.5 weight ratio for PST-18NR or TiO₂ paste : ethanol = 2:7 weight ratio for PST-30NRD), followed by heating the substrates at 550 °C for 30 min. For some TA measurements, glass, instead of FTO was used as the substrate and a porous Y₂O₃ layer was fabricated on the glass substrates. Next, CH₃NH₃I and PbCl₂ were mixed with a 3:1 molar ratio for preparing a 40 % solution of perovskite in N,N-dimethylformamide and the mixture was spin-coated on the TiO₂ and Y₂O₃ porous substrates. After heating at 100 °C for 45 minutes,

the substrates were spin-coated with a mixture of 55 mM of tert-butylpyridine, 9 mM of lithium bis(trifluoromethylsulfonyl)imide salt, and 68 mM of *spiro*-OMeTAD. Finally, Ag and Au electrodes were fabricated by vacuum deposition for the photovoltaic measurements. The photovoltaic performance was evaluated using an AM1.5G 100 mW/cm² irradiance solar simulator (CEP-2000, Bunkoukeiki Inc) with a 0.4 cm x 0.4 cm mask.

The Sn/Pb cocktail perovskite samples were prepared using the following method. [23] PbI₂ (Purity: 99.999 %), SnI₂, and regioregular poly(3-hexylthiophene-2,5-diyl) (P3HT) were purchased from Sigma Aldrich and used as received. F-doped SnO₂ coated glass (FTO glass), Nippon Sheet Glass Co. Ltd) was patterned using Zn and a 6 N HCl aqueous solution. A compact TiO₂ layer was produced by spraying titanium diisopropoxide bis(acetylacetonate) solution in ethanol onto this patterned glass at 300 °C. The substrate was then dipped in a 40 mM solution of TiCl₄ in water for 30 min. Then the substrate was baked at 500 °C for 20 min. Next, a porous TiO₂ layer was produced by spin-coating with a TiO₂ paste (PST-18NR, JGC Catalysts and Chemicals Ltd.) in ethanol (TiO₂ paste : ethanol = 2:7 weight ratio). The substrate was then heated at 550 °C for 30 min. For certain TA measurements, glass substrates other than FTO ones, with a porous Al₂O₃ layer deposited on them, were used. The substrates were then spin-coated with a mixture of SnI₂, PbI₂, and CH₃NH₃I (0.5 : 0.5 : 1.0 (molar ratio)) in dimethylformamide (DMF) (40 wt %), and they were baked at 70 °C for 30 min. Next, P3HT in chlorobenzene solution (15 mg/ml) was spin-coated on the prepared perovskite layer and the substrate was put in nitrogen at ambient temperature for 1 h. For conducting TA measurements, samples of Sn/Pb cocktail perovskite deposited on both Al₂O₃ and TiO₂ substrates with and without P3HT as a hole transport material (HTM) were employed. Ag and Au electrodes were finally deposited by vacuum deposition for characterizing the photovoltaic performance, which was evaluated using an AM 1.5G 100 mW/cm² irradiance solar simulator (CEP-2000SRR, Bunkoukeiki Inc) with a 0.4 cm x 0.4 cm mask.

2.2. Characterization methods

2.2.1. Optical absorption measurements

A gas-microphone photoacoustic (PA) technique [26] was used to study the optical absorption properties of the samples. The light source was a 300 W xenon arc lamp. By passing the light through a monochromator, a monochromatic light beam was obtained. This beam was modulated with a mechanical chopper and focused onto the surface of the sample placed in a sealed PA cell filled with N₂ gas. The measurements of PA spectrum were carried out in the wavelength range of 500–1200 nm with a modulation frequency of 33 Hz at room temperature. The PA signal was measured by first passing the microphone output through a preamplifier and then to a lock-in amplifier. The PA spectra were normalized with the PA spectrum obtained from a carbon black sheet.

2.2.2. Transient Absorption (TA) Measurements

Two different TA setups were used: the charge separation (electron injection and hole injection) dynamics was characterized by a femtosecond TA technique (fs-TA) [27, 28] and charge

recombination dynamics was characterized by a nanosecond TA technique (ns-TA) [28-31]. In the fs-TA setup for characterizing the charge separation, [27, 28, 31] the laser source used was a titanium/sapphire laser (CPA-2010, Clark-MXR Inc.) with a wavelength of 775 nm, a repetition rate of 1 kHz, and a pulse width of 150 fs. The light was separated into two parts. One part was used as a probe pulse. The other part was used to pump an optical parametric amplifier (OPA) (a TOAPS from Quantronix) to generate light pulses with a wavelength tunable from 290 nm to 3 μm . This was used as a pump light to excite the sample. In this study, a pump light wavelength of 470 nm and a probe beam wavelength of 775 nm were used. Deschler and co-workers [32] reported very recently that the TA response of ground state bleaching (GSB) for $\text{CH}_3\text{NH}_3\text{PbCl}_2$ on glass peaked at 1.65 eV and was spectrally unchanged up to times beyond 200 ns. Therefore, the probe light wavelength of 775 nm (i.e., the photon energy of 1.64 eV) used in this study is appropriate to monitor the GSB of $\text{CH}_3\text{NH}_3\text{PbCl}_2$ on Y_2O_3 and TiO_2 substrates with or without *spiro*-OMeTAD, and thus electron transfer and hole transfer processes at each interface can be investigated systematically. On the other hand, in the case of Sn/Pb cocktail perovskite, the probe light of 775 nm was used to detect the photo-excited carrier absorption.

In the ns-TA setup for characterizing the charge recombination [28-31], the pump light source was an OPO (Surelite II – 10FP) output excited by a Nd:YAG nanosecond pulse laser (Panther, Continuum, Electro-Optics Inc.), with a pulse width of 5 ns and a repetition rate of 0.5 Hz. A pulse light with a wavelength of 470 nm was used as the pump light to excite the sample. The probe light was produced from a fiber coupled CW semiconductor. Three different probe wavelengths, of 785 nm, 658 nm and 1310 nm, were used. Specifically, the probe beam of 785 nm was employed to measure the TA responses of GSB for MAPbCl_2 on Y_2O_3 substrates, i.e., the recombination of electrons and holes in MAPbCl_2 . [32] The probe beam of 658 nm was used to measure the trapped electrons in TiO_2 [33] based on the research of Yoshihara and co-workers, which was used to investigate charge recombination between the electrons in TiO_2 and the holes in the perovskite. The probe beam of 1310 nm was used to monitor the holes in *spiro*-OMeTAD [34] and thus measure the charge recombination between holes in *spiro*-OMeTAD and electrons in TiO_2 and/or in perovskite. For all measurements, the pump and probe lights were irradiated from the glass side and the TA measurements were carried out in a nitrogen atmosphere.

3. Optical Absorption Study: Bandgap and Urbach Energy of Pb and Sn/Pb cocktail perovskite

Figure 1 shows the optical absorption spectra of the Pb (MAPbI_2) and Sn/Pb cocktail ($\text{MASn}_{0.5}\text{Pb}_{0.5}\text{I}_3$) perovskite samples on a porous TiO_2 substrate measured using the PA technique (we refer to this as the PA spectrum in the following) at room temperature. From the position of the shoulder in each PA spectrum, [35] the bandgap energies of MAPbI_2 and $\text{MASn}_{0.5}\text{Pb}_{0.5}\text{I}_3$ are determined to be 1.52 and 1.21 eV, respectively, which are almost the same as those given in our earlier reports. [23, 25] We find that, below the shoulder, the trend of the absorption coefficient is exponential. The slope of this exponential tail, known as the Urbach

tail, corresponds to the absorption tail states, and is usually quantitatively expressed by the Urbach Energy E_U . [18, 31, 36] Investigation of these exponential tails can offer important information on the band structure, disorder, defects, impurities, and electron-phonon interactions in semiconductor materials. The numerical relationship between the optical absorption coefficient α in the exponential tail and the photon energy ($h\nu$) is shown in eq. (1), through which the values of E_U of the samples can be calculated. [37, 38]

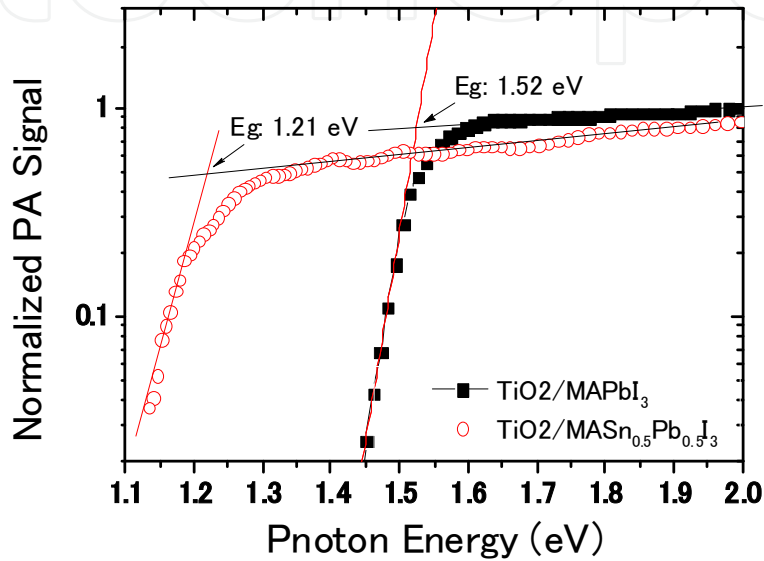


Figure 1. Optical absorption spectra of MAPbI₃ and Sn/Pb cocktail MASn_{0.5}Pb_{0.5}I₃ perovskite measured using a photoacoustic (PA) technique. The bandgap energies were determined to be 1.52 eV and 1.21 eV, respectively. The Urbach energies were determined to be 22 meV and 34 meV, respectively.

$$\alpha = \alpha_0 \exp\left(\frac{h\nu - h\nu_0}{E_u}\right) \quad (1)$$

where h is Planck's constant, and α_0 , ν_0 , E_u are fitting parameters. The values of E_u for Pb and Sn/Pb cocktail perovskites were determined to be 22 meV and 34 meV, respectively. The value of E_u for Sn/Pb cocktail perovskite is larger than that for the Pb perovskite. It can be assumed that the value of E_u is a reflection of the disorder and/or defects in the semiconductor crystal. [18, 36-38] Thus, the width of the exponential tail increases with increasing density of defects. Therefore, the larger E_u determined for Sn/Pb cocktail perovskite (i.e., 34 meV) implies that there could be higher defect states in the sample compared to MAPbI₃ (i.e., 22 meV). This will lead to faster recombination of photoexcited carriers in the Sn/Pb cocktail MASn_{0.5}Pb_{0.5}I₃ perovskite and lower values of V_{oc} and FF , which we will discuss in detail below together with the TA measurement results.

4. Dynamics of Photoexcited Carrier Recombination and Charge Transfer in Pb-based Perovskite Solar Cells and their Relationships to the Photovoltaic Properties^[25, 39, 40]

To perform systematic investigations on the charge separation and recombination dynamics in perovskite solar cells, TA measurements were conducted for MAPbI₃ on either Y₂O₃ or TiO₂ substrates, with and without a *spiro*-OMeTAD layer. For perovskite deposited on Y₂O₃ substrate, the lifetime of photoexcited charge carriers in MAPbI₃ and the charge separation dynamics at the MAPbI₃/*spiro*-OMeTAD interface were studied by the fs-TA technique. The pump light wavelength used to excite MAPbI₃ only was 470 nm, and the probe light wavelength used was 775 nm, which is just at the optical absorption edge of MAPbI₃. Figure 2 shows the normalized TA response of MAPbI₃/Y₂O₃ for a time scale of up to 3 ns with a lower pump light intensity (0.9 μJ/cm²) with and without the *spiro*-OMeTAD layer. We can observe a bleaching signal with a very slow decay in the figure. Because electron injection from the perovskite to Y₂O₃ cannot occur due to the large band gap of Y₂O₃, it is reasonable to attribute the slow decay to the slow recombination process of photoexcited charge carriers in MAPbI₃. Two processes were found in the TA decay process and the TA signal obtained can be fitted to the biexponential function shown below very well:

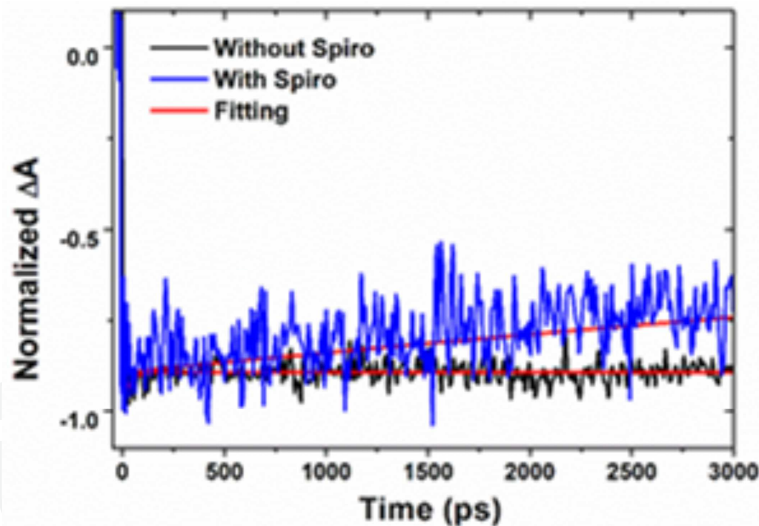


Figure 2. Normalized TA responses of MAPbI₃/Y₂O₃ with and without *spiro*-OMeTAD as a hole transport material (HTM). The red solid lines represent the fitting results with eq. (2). (reference: 25)

$$Y = A_1 e^{-t/t_1} + A_2 e^{-t/t_2} \quad (2)$$

where t_1 and t_2 are two time constants, A_1 and A_2 are the contributions from the corresponding components. The time constants t_1 and t_2 of the two charge recombination processes were calculated to be 34 ps ($A_1/(A_1+A_2)$: 9%) and much larger than 10 ns ($A_2/(A_1+A_2)$: 91%), respec-

tively. The faster decay process could be attributed to nonradiative recombination of electrons and holes through defects or trap states in MAPbI₃ or at the MAPbI₃/Y₂O₃ interface. The relative contribution of the faster decay is less than 10%, which suggests that the defect or trap state density in MAPbI₃ or at the interface is very small, which is consistent with a thermally stimulated current measurement. [39, 40] The slower decay process could be attributed to the recombination of free electrons and holes in MAPbI₃. This result suggests that the lifetime of the photoexcited charge carriers was very long, which was confirmed to be as much as the order of microseconds by the ns-TA measurement results shown in Figure 3. The TA decay was fitted with eq. (2), and two decay processes were found with lifetimes of 3.7±0.1 μs (70%) and 60±1 μs (30%), respectively. Combining the fs-TA and ns-TA results for MAPbI₃/Y₂O₃, the lifetime of the photoexcited charge carriers in MAPbI₃ can be mostly considered to be as long as the order of microseconds.

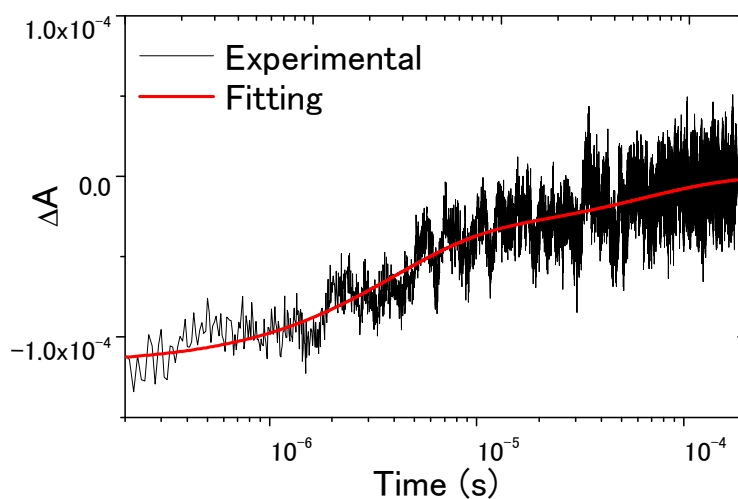


Figure 3. TA responses of MAPbI₃/Y₂O₃ without *spiro*-OMeTAD for a time scale of 200 μs measured with a pump light wavelength of 470 nm and a probe light wavelength of 785 nm. The red solid lines represent the fitting results with eq. (2). (reference: 25)

The TA response of MAPbI₃/Y₂O₃ with *spiro*-OMeTAD was fitted to eq. (2), and only one exponential decay with a time constant of 16±2 ns was found. Compared with the long lifetime of the TA decay in Y₂O₃/MAPbI₃, the fast decay process in Y₂O₃/MAPbI₃/*spiro*-OMeTAD can be considered to originate from the photoexcited hole injection from MAPbI₃ to *spiro*-OMeTAD. This result indicates that charge separation occurred at the interface between MAPbI₃ and *spiro*-OMeTAD. [25]

Figure 4 shows the TA response of MAPbI₃/Y₂O₃ with a layer of *spiro*-OMeTAD measured at a probe wavelength of 1310 nm. This result clearly indicates that charge separation at the MAPbI₃/*spiro*-OMeTAD interface truly occurred, which is entirely consistent with the fs-TA results shown in Figure 2. The decrease of the TA signal in the sample of MAPbI₃/Y₂O₃ with a layer of *spiro*-OMeTAD originated from the recombination process between the electrons in MAPbI₃ and the holes in *spiro*-OMeTAD, which can be fitted very well with eq. (2). Only one exponential decay process was observed, with a time constant determined to be 0.37±0.07 μs,

which corresponds to the recombination time [25]. Figure 5 shows the photoexcited charge carrier (electrons and holes) dynamics in MAPbI₃ deposited on a Y₂O₃ substrate with *spiro*-OMeTAD as a HTM.

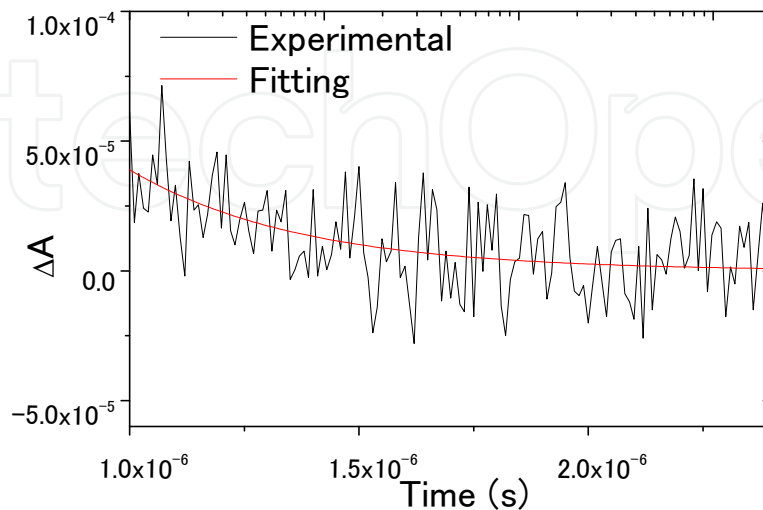


Figure 4. TA responses of MAPbI₃/Y₂O₃ with *spiro*-OMeTAD measured with a pump light wavelength of 470 nm and a probe light wavelength of 1310 nm. The red solid lines represent the fitting results with eq. (2). (reference: 25)

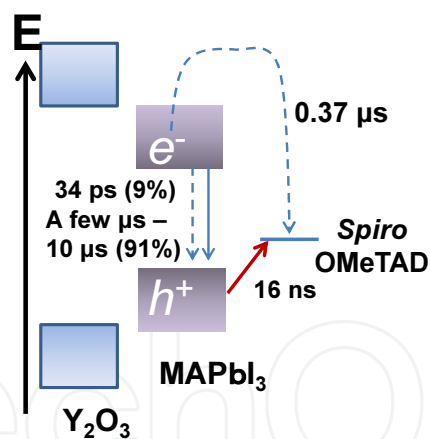


Figure 5. Schematic illustration of photoexcited charge carrier (electrons and holes) dynamics in MAPbI₃ deposited on a Y₂O₃ substrate with *spiro*-OMeTAD as a HTM. (reference: 25)

The photoexcited electron injection and the recombination dynamics were measured using the TA techniques for MAPbI₃ deposited on TiO₂ substrates. Figure 6(a) shows the normalized TA responses of MAPbI₃/TiO₂ for 400 ps measured with different pump light intensities. The decay processes in the normalized TA responses overlapped very well with each other when the pump light intensity was lower. However, when the pump light intensity became larger than 3.75 μJ/cm², a faster decay process, resulting from Auger recombination, appeared in the TA response. [25] To determine the electron injection dynamics from MAPbI₃ to TiO₂, the TA

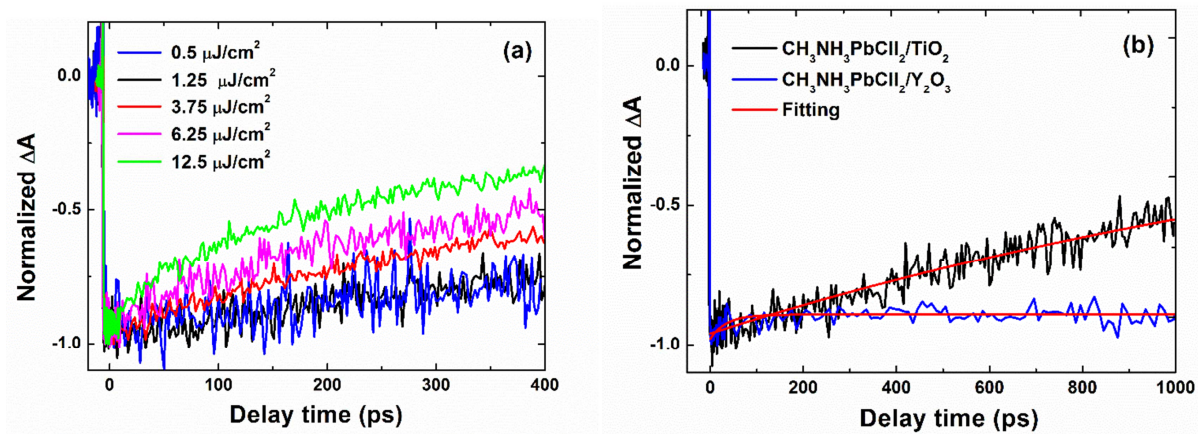


Figure 6. (a) Dependence of the normalized TA responses of $\text{CH}_3\text{NH}_3\text{PbCl}_2/\text{TiO}_2$ on pump light intensity and (b) theoretical fitting results of the TA response (pump light intensity: 1.25 $\mu\text{J}/\text{cm}^2$) with a biexponential function (eq. (2)). For comparison, the TA response of $\text{CH}_3\text{NH}_3\text{PbCl}_2/\text{Y}_2\text{O}_3$ is also shown in (b). The pump light wavelength is 470 nm and the probe light wavelength is 775 nm. (reference: 25)

response of $\text{MAPbI}_3/\text{TiO}_2$ measured under a lower pump light intensity (0.9 $\mu\text{J}/\text{cm}^2$) was used to make a comparison with that of $\text{MAPbI}_3/\text{Y}_2\text{O}_3$ as shown in Figure 6(b). The TA response of $\text{MAPbI}_3/\text{TiO}_2$ decayed much faster than that of $\text{MAPbI}_3/\text{Y}_2\text{O}_3$ and can be fitted to a single exponential decay function very well, with a time constant determined to be 1.8 ± 0.1 ns, which is approximately 2 - 3 orders smaller than the photoexcited charge carrier lifetimes ($\sim \mu\text{s}$) of MAPbI_3 as shown above. Then the electron injection time t_{ET} and electron injection rate k_{ET} were calculated to be about 1.8 ns and $5.5 \times 10^8 \text{ s}^{-1}$, respectively. [25] Thus, the electron injection efficiency η_{Einj} was calculated to be about 100% for all electrons with lifetimes longer than 100 ns. It is supposed here that the other 9% of charge carriers that recombined with a lifetime of 34 ps were not present in the MAPbI_3 prepared on TiO_2 , because no faster decay component was observed in the TA responses of $\text{MAPbI}_3/\text{TiO}_2$. [25]

Next, the recombination dynamics in $\text{MAPbI}_3/\text{TiO}_2$ without the layer of *spiro*-OMeTAD, i.e., the recombination process between the electrons in TiO_2 and the holes in MAPbI_3 was measured using ns-TA. Figure 7 shows the TA response of $\text{MAPbI}_3/\text{TiO}_2$ measured with a pump light wavelength of 470 nm and a probe light wavelength of 658 nm. [25] According to the TA signal in nanocrystalline TiO_2 films reported by Yoshikawa [33] and our earlier studies, [18-21] it is reasonable to think that the TA response in $\text{MAPbI}_3/\text{TiO}_2$ observed at 658 nm corresponds to the electrons in TiO_2 injected from MAPbI_3 . [25] Then the recombination time between the electrons in TiO_2 and the holes in perovskite was determined to be 0.14 μs by fitting Figure 7 to eq. (2).

Then, the recombination dynamics in $\text{MAPbI}_3/\text{TiO}_2$ with *spiro*-OMeTAD as a hole transport material, i.e., the recombination between the electrons in TiO_2 and the holes in *spiro*-OMeTAD, were measured using ns-TA. Figure 8 shows the TA responses of $\text{MAPbI}_3/\text{TiO}_2$ without and with *spiro*-OMeTAD, which were measured with a pump light wavelength of 470 nm and a probe light wavelength of 1310 nm, which was used to monitor the relaxation dynamics of holes in *spiro*-OMeTAD. From fig. 8 we can see that no TA signal was observed for the

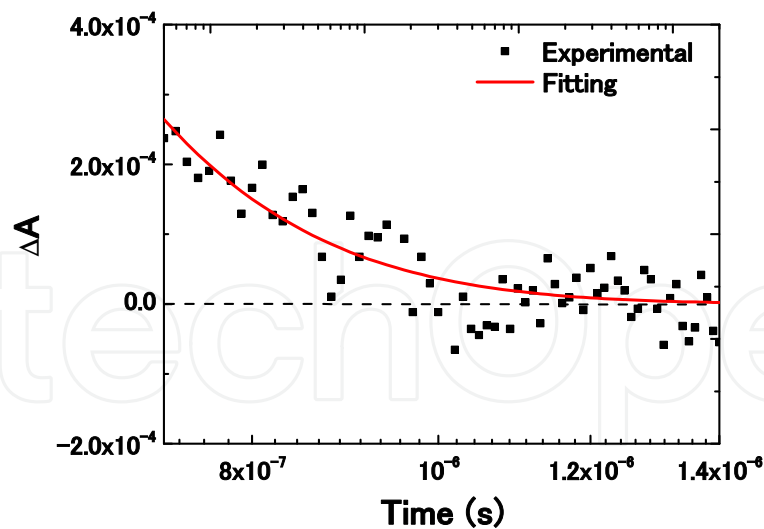


Figure 7. TA response of MAPbI₃/TiO₂ without a HTM measured with a pump light wavelength of 470 nm and a probe light wavelength of 658 nm. The red solid line represents the fitting result with a single exponential decay function with a time constant of 0.14 μs. (reference: 25)

sample without *spiro*-OMeTAD. However, for the sample with *spiro*-OMeTAD, an absorption signal can be clearly observed, which confirms that the TA signal probed at 1310 nm originated from the holes in *spiro*-OMeTAD. The TA decay in Figure 8 can be fitted very well with a single exponential decay function and the time constant was determined to be 60 ± 0.5 μs. This is a typical result for cells with 18 nm sized TiO₂ nanoparticles. It is important to understand how the carrier dynamics relate to the photovoltaic properties of the cells. Several cells were measured and the energy conversion efficiency was typically 5-7%. These cells are called cell A.

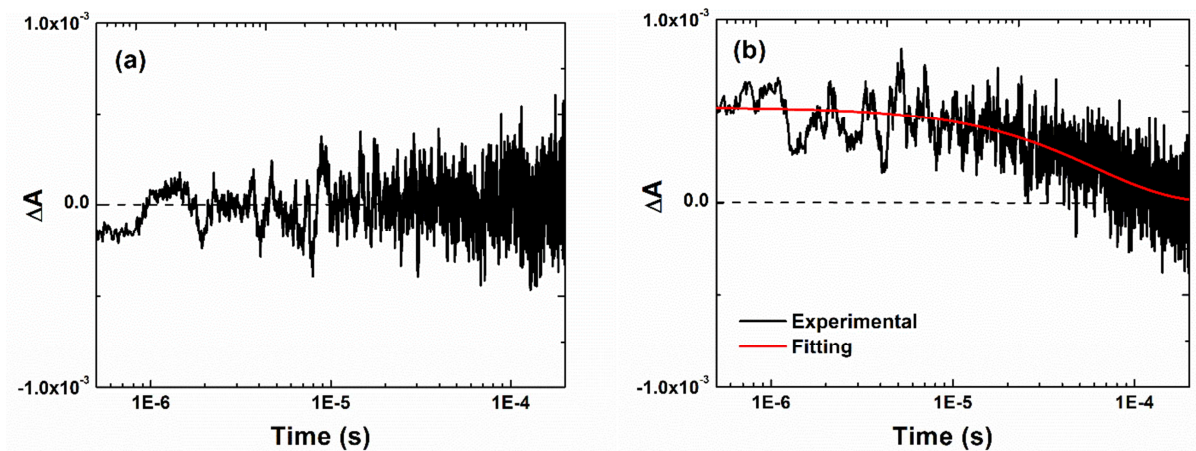


Figure 8. TA responses of MAPbI₃/TiO₂ without (a) and with (b) *spiro*-OMeTAD as a HTM measured with a pump light wavelength of 470 nm and a probe light wavelength of 1310 nm. The red solid line in (b) represents the fitting result with a single exponential decay function with a time constant of 60 μs. (reference: 25)

Then another kind of cell with 30 nm sized TiO_2 nanoparticles were also studied, which we call cell B. The energy conversion efficiency of cell B was typically 8-10%. It was found that the recombination dynamics in the Perovskite solar cells has a great influence on the IPCE, J_{sc} and the energy conversion efficiency. [25] Two kinds of $\text{TiO}_2/\text{MAPbI}_3/\text{spiro-OMeTAD}$ solar cells showing different IPCE spectra and photovoltaic performance were studied, and the relationships between the charge separation and recombination dynamics and the photovoltaic properties were investigated. [25] Figure 9 shows the IPCE spectra and current-voltage (I-V) curves of the two kinds of cell. For cells A and B, the TiO_2 mesoporous layers were made of TiO_2 nanoparticles with sizes of 18 nm and 30 nm, respectively. The short circuit current J_{sc} , open circuit voltage V_{oc} , fill factor FF and energy conversion efficiency η of cell A are 11.81 mA/cm^2 , 0.79 V, 0.71 and 6.59%, respectively. The IPCE value at 470 nm (the pump light wavelength used in the TA measurements) is 58%. On the other hand, for cell B, J_{sc} , V_{oc} , FF and η are 17.60 mA/cm^2 , 0.78 V, 0.69 and 9.54%, respectively. The IPCE value of cell B at 470 nm is about 85%. To investigate the correlation between the photoexcited charge carrier dynamics and the photovoltaic properties, especially the IPCE, the charge separation and recombination dynamics of cell B were also characterized [25]. Figure 10 compares the charge carrier dynamics of the two cells A and B, it can be seen that the recombination time of electrons in TiO_2 and holes in the perovskite was almost identical (i.e., 0.13-0.14 μs), and the electron injection time was a little faster (0.7 ns) in cell B. However, the recombination time of electrons in TiO_2 and holes in *spiro-OMeTAD* in cell B became as long as 600 μs , which is ten times longer than that in cell A (60 μs). It is important to see how these changed separation and recombination dynamics influence the IPCE and J_{sc} of the two kinds of cell. It is well known that IPCE is proportional to the charge separation efficiency η_{Csep} and the charge collection efficiency η_{Ccol} , where η_{Csep} is the product of the electron injection efficiency η_{Einj} and the hole injection efficiency η_{Hinj} . η_{Einj} , η_{Hinj} and η_{Ccol} can be calculated using the photoexcited carrier lifetimes, electron and hole injection times, and recombination times as shown in Figures 5 and 10. As discussed in detail in reference 25, the charge separation efficiency of the two kinds of cell were found to be almost the same, about 90%. However, the charge collection efficiency of cell B was found to be almost 100%, which is much larger than that of cell A, only 70%.

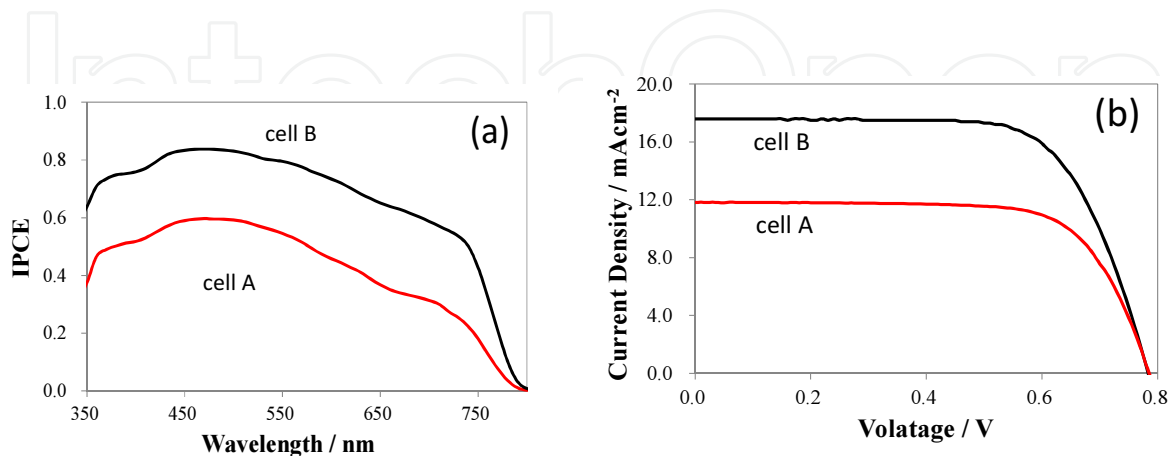


Figure 9. Incident photon to current conversion efficiency (IPCE) spectra of the solar cells A (red) and B (black) (a) and current voltage (I-V) curves of $\text{TiO}_2/\text{MAPbI}_3/\text{spiro-OMeTAD}$ solar cells A (red) and B (black) (b). (reference: 25)

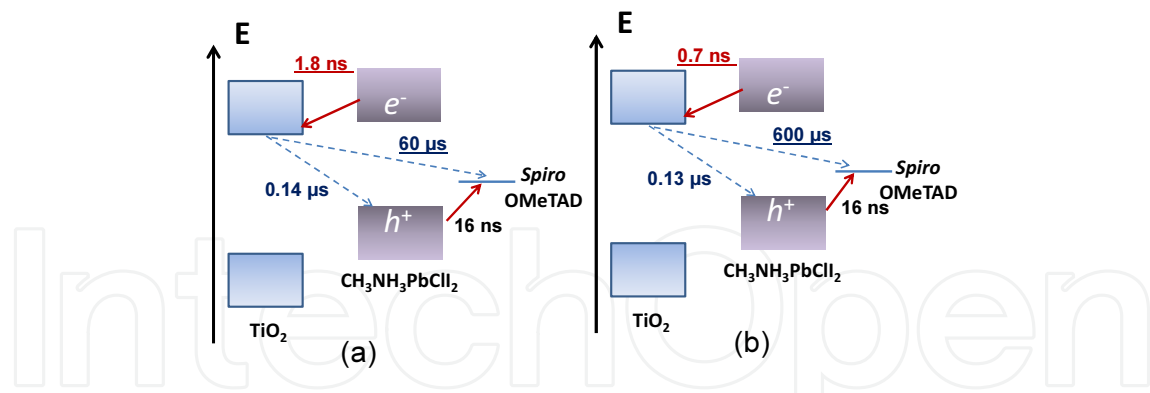


Figure 10. Schematic illustration of photoexcited electron injection and recombination dynamics in two $\text{TiO}_2/\text{MAPbI}_3/\text{spiro-OMeTAD}$ solar cells A (a) and B (b). (reference: 25)

5. Dynamics of Photoexcited Carrier Recombination and Charge Transfer in Sn/Pb Cocktail Perovskite Solar Cells and their Relationships to the Photovoltaic Properties^[31]

To find the mechanism responsible for the low PCE, especially the low V_{oc} and FF in Sn/Pb cocktail perovskite solar cells, which has been reported [23], both the fs-TA and ns-TA techniques were used to investigate the charge separation and recombination dynamics in these solar cells systematically. [31] Sn/Pb cocktail perovskites deposited on either Al_2O_3 or TiO_2 films, with and without P3HT, were measured by the TA techniques using probe beams with different wavelengths. Similar to the Pb-based perovskite solar cells discussed above, firstly, photoexcited carrier lifetimes, hole injection to P3HT and recombination at the Sn/Pb cocktail perovskite/P3HT interface were clarified as shown in Figure 11. [31] The photoexcited carrier lifetimes are 4.2 ± 0.4 ps ($A_1/(A_1+A_2+y_0)$: 55%), 650 ± 57 ps ($A_2/(A_1+A_2+y_0)$: 25%), and much longer than 3 ns ($y_0/(A_1+A_2+y_0)$: 20%), respectively. Therefore, the recombination dynamics and lifetimes of photoexcited carriers in Sn/Pb cocktail perovskite are much faster and shorter than those in Pb-based perovskite, for which case they are much greater than 100 ns for over 90% of the photoexcited carriers as mentioned above. It is considered that the faster decay processes are due to some nonradiative recombination of electrons and holes through defects or trap states in the Sn/Pb cocktail perovskite, which is consistent with the measured larger Urbach energy in the Sn/Pb cocktail perovskite (i.e., 34 meV). It is larger than that in Pb-based perovskite (i.e., 22 meV). On the other hand, the charge separation at the interface between Sn/Pb cocktail perovskite and P3HT occurred in approximately 1 ps and interfacial charge recombination between the Sn/Pb cocktail perovskite (on an Al_2O_3 substrate) and P3HT occurred in approximately 16 ps. [31]

Secondly, the photoexcited charge separation and recombination dynamics of Sn/Pb cocktail perovskite deposited on a TiO_2 substrate with P3HT as a hole transport material were evaluated, which is shown in Figure 12. The charge separation at the perovskite/ TiO_2 interface occurs in as fast as 1 ps. It is worth noting that the recombination time at the Sn/Pb cocktail perovskite/

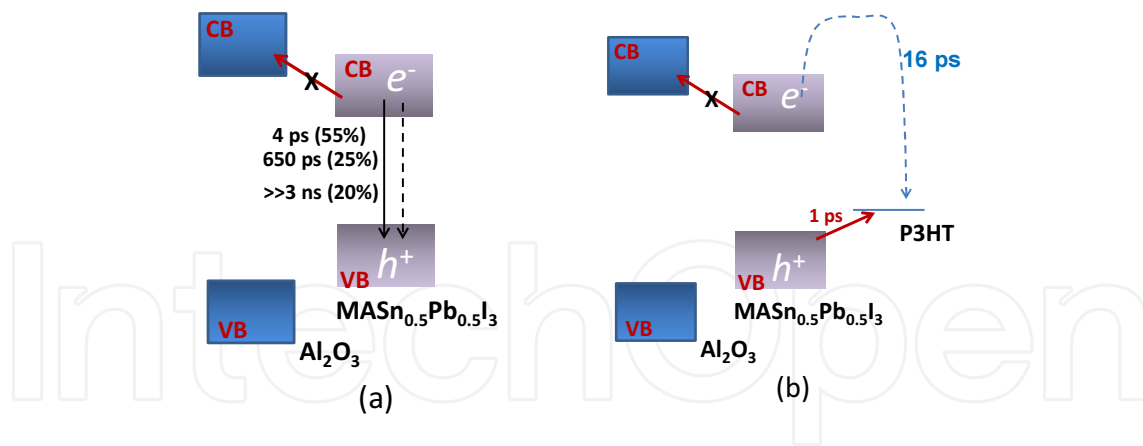


Figure 11. Schematic illustration of photoexcited charge carrier (electrons and holes) dynamics in Sn/Pb cocktail $\text{MASn}_{0.5}\text{Pb}_{0.5}\text{I}_3$ perovskite deposited on an Al_2O_3 substrate without (a) and with (b) P3HT as a hole transport material. (reference: 31)

TiO_2 interface is $880 \mu\text{s}$, which is about two to three orders of magnitude slower compared to that occurring at the $\text{MAPbI}_3/\text{TiO}_2$ interface as shown in Figure 10. On the other hand, the recombination time at the $\text{TiO}_2/\text{P3HT}$ interface is $190 \mu\text{s}$, which is much faster compared to that without P3HT. This indicates that the recombination of electrons in the TiO_2 becomes faster when P3HT is used, which originates from the recombination at the $\text{TiO}_2/\text{P3HT}$ interface. This recombination is one of the main reasons for the lower V_{oc} and FF of the Sn/Pb cocktail solar cells. [23] Pinhole-free Sn/Pb cocktail perovskite needs to be prepared in order to reduce direct interaction between the TiO_2 and P3HT, thus suppressing potential recombination. [31]

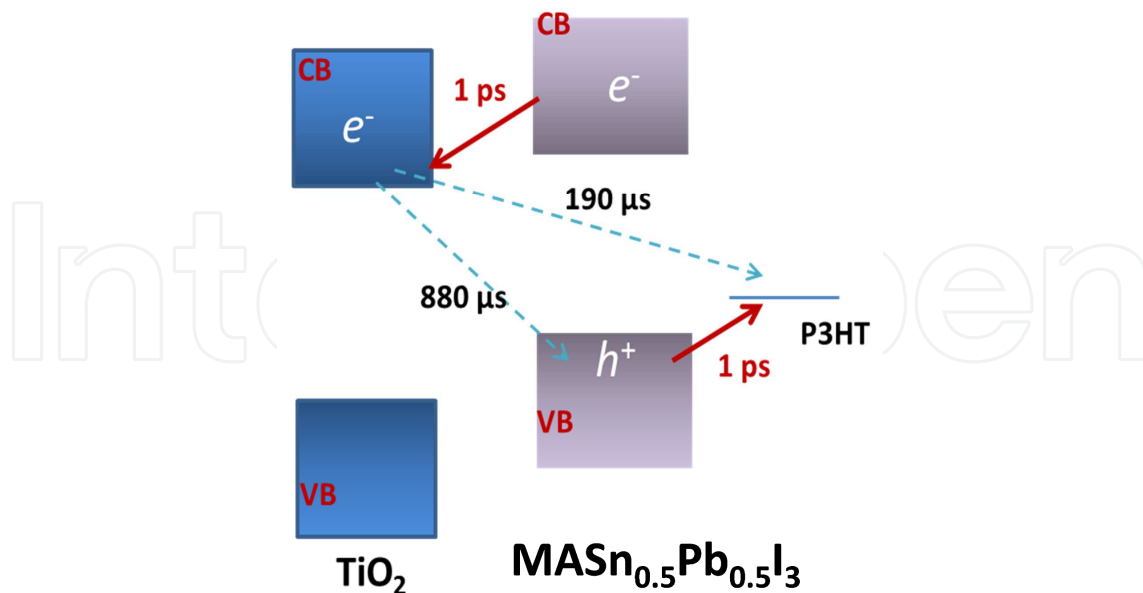


Figure 12. Schematic illustration of photoexcited charge separation and recombination dynamics in Sn/Pb cocktail $\text{MASn}_{0.5}\text{Pb}_{0.5}\text{I}_3$ perovskite solar cells with TiO_2 as an electron transport material (ETM) and P3HT as a HTM. (reference: 31)

It is important to understand how the optical absorption, charge separation and recombination dynamics relate to the incident photon to current conversion efficiency (IPCE) spectrum and the current-voltage (I-V) characteristics of the solar cell. Figure 13 shows a typical IPCE spectrum of a Sn/Pb cocktail perovskite solar cell. Based on the photoexcited carrier relaxation dynamics of Sn/Pb perovskite on an Al_2O_3 substrate, and the charge transfer dynamics at TiO_2 /perovskite/P3HT interfaces, which are summarized in Table 1, it is possible to calculate the charge separation efficiency. [31] First, it is determined that the hole injection efficiency η_{Hinj} is almost 100% and the electron injection efficiency η_{Einj} is about 86%. Thus, the charge separation efficiency η_{Csep} ($\eta_{\text{Csep}} = \eta_{\text{Hinj}}\eta_{\text{Einj}}$) is 86%. The 14% loss in η_{Csep} results from the fast recombination component, with a lifetime of 4 ps, of photoexcited carriers in the Sn/Pb cocktail perovskite, which may originate from the nonradiative recombination owing to the defects in the sample. Therefore, in order to achieve 100% charge separation efficiency, the crystalline quality of the Sn/Pb cocktail perovskite has to be improved. The optical absorption is estimated to be about 95% in this case, due to the fact that the perovskite material is much more absorbing over a broader range up to 1000 nm, which could result in complete absorption (such as at 470 nm) in thin films such as 500 nm. [23] As shown in Figure 13, the IPCE value at 470 nm, corresponding to the excitation wavelength used for the TA measurements, is 68%. So the charge collection efficiency η_{Ccol} is estimated to be 83%. [31] The 17% loss in η_{Ccol} mainly originates from the charge recombination occurring at the TiO_2 /P3HT interface. In order to improve IPCE and J_{sc} for the solar cell, direct contact between P3HT and TiO_2 should be avoided or at least suppressed by preparing a pinhole-free Sn/Pb cocktail perovskite layer on TiO_2 or by inserting a barrier/blocking layer at the interface. [31]

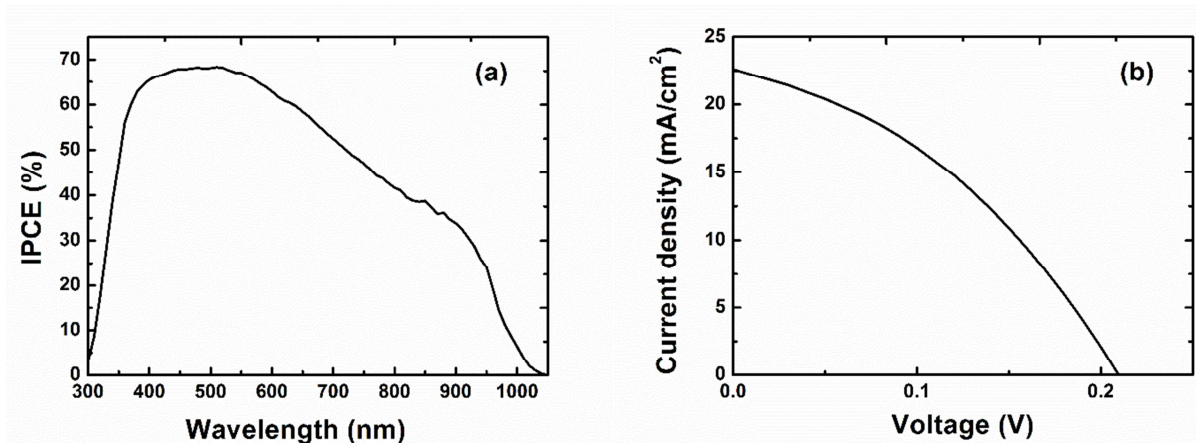


Figure 13. A typical incident photon to current conversion efficiency (IPCE) spectrum (a) and current-voltage (I-V) curve (b) of a Sn/Pb cocktail $\text{MASn}_{0.5}\text{Pb}_{0.5}\text{I}_3$ perovskite solar cell.(reference: 31)

As shown in Figure 13(b), J_{sc} , V_{oc} , FF and PCE of the Sn/Pb cocktail perovskite solar cells are 22.61 mA/cm^2 , 0.21 V, 0.37 and 1.77%, respectively. It is obvious that the low PCE is mainly due to the low V_{oc} and FF. J_{sc} could be improved to as high as 30 mA/cm^2 if the charge separation efficiency can be increased to 100% by reducing the fast nonradiative recombination rate and if the charge collection efficiency can be increased to more than 95% through suppression of

Samples	Al ₂ O ₃ / MASn _{0.5} Pb _{0.5} I ₃	Al ₂ O ₃ / MASn _{0.5} Pb _{0.5} I ₃ / P3HT	TiO ₂ / MASn _{0.5} Pb _{0.5} I ₃	TiO ₂ / MASn _{0.5} Pb _{0.5} I ₃ / P3HT
Charge separation	N/A	Hole injection 1 ps	Electron injection 1 ps	Electron/hole injections 1 ps/1 ps
Bulk recombination (photoexcited carrier lifetimes)	4 ps (55%) 650 ps (25%) >>3 ns (20%)	N/A	N/A	N/A
Interfacial recombination	N/A	16 ps	880 μs	190 μs

Table 1. Photoexcited carrier lifetimes, hole injection and electron injection dynamics as well as charge recombination at each interface in MASn_{0.5}Pb_{0.5}I₃ perovskite solar cells. [31]

the recombination occurring at the TiO₂/P3HT interface. For V_{oc} the bandgap-voltage offset $E_G - qV_{oc}$ is calculated to be as large as 1 eV, where E_G is the bandgap of 1.21 eV and q is the elementary charge. This bandgap-voltage offset is quite similar to that of amorphous silicon, and is thought to be closely related to the larger Urbach energy as shown in Figure 14. The recombination resistance from the I-V curve was estimated to be 27 Ω cm², which could also result in a lower V_{oc} . The smaller recombination resistance estimated is mostly due to the faster recombination of electrons and holes at the TiO₂/P3HT interface. Thus, the lower V_{oc} in the Sn/Pb cocktail perovskite solar cells is due to two reasons: (1) the larger Urbach energy; (2) the smaller recombination resistance. The lower FF is also due to reason (2). Therefore, these findings imply that the photovoltaic performance of the Sn/Pb cocktail perovskite solar cells can be further improved by decreasing the Urbach energy, i.e., reducing the defects in the perovskite, and by reducing the recombination occurring at the TiO₂/P3HT interface through appropriate interface engineering such as passivation or inserting a barrier/blocking layer. [31]

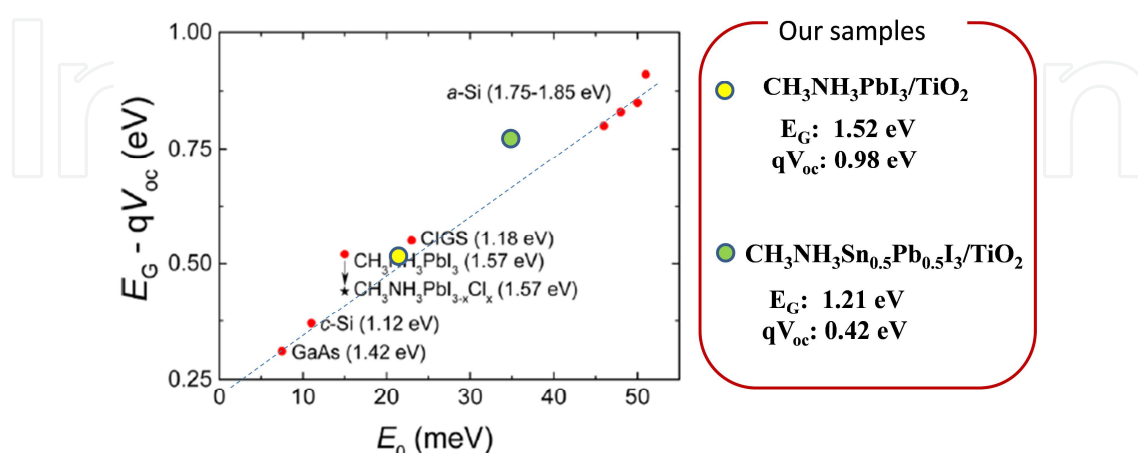


Figure 14. The bandgap-voltage offset ($E_G - qV_{oc}$) versus Urbach energy for typical photovoltaic absorber materials (from reference 18) and for the Pb and Sn/Pb cocktail perovskites used in our study at room temperature.

6. Conclusions

In summary, by conducting a systematic study on the optical absorption, photoexcited charge carrier lifetimes, and charge separation and charge recombination dynamics, we have explored the ways through which the photovoltaic performance of Pb and Sn/Pb cocktail perovskite solar cells can be improved.

For MAPbI₃ solar cells, we find that the great differences in the IPCE and J_{sc} of the two kinds of cell result from the great difference in the charge recombination between the electrons in TiO₂ and holes in *spiro*-OMeTAD. These results indicate that the key for improving the IPCE and J_{sc} of the perovskite-based solar cells is charge collection efficiency, instead of charge separation efficiency. Thus suppressing the recombination through proper interfacial engineering for perovskite-based solid hybrid solar cells is crucial for achieving a high efficiency.

For the Sn/Pb cocktail perovskite solar cells, it is determined that the bandgap is 1.21 eV and light harvesting can be extended to a wider wavelength over 1000 nm. The Urbach energy is calculated to be 34 meV, which is more than twice that of the MAPbI₃ perovskite. Three recombination processes for the photoexcited carriers were found with lifetimes being 4 ps (55%), 650 ps (25%) and one much larger than 3 ns (20%). The larger Urbach energy and the faster recombination suggest that there are defects in the prepared Sn/Pb cocktail perovskite. These results are significantly different from those of the MAPbI₃ perovskite, in which case the photocarrier lifetimes are larger than 100 ns and almost no defects were observed. Moreover, the charge separation and charge recombination dynamics were explored. We find that both the electron injection into TiO₂ and hole transfer to the P3HT layer occurred on a timescale of 1 ps. It was surprising to find that the charge recombination lifetime at the Sn/Pb cocktail perovskite/TiO₂ interface was as long as 880 μ s, which is 2-3 orders of magnitude greater than that occurring at the MAPbI₃/TiO₂ interface. However, the charge recombination lifetime became shorter, i.e., 190 μ s, when P3HT was employed as a HTM. This implies that the charges can be more effectively collected without the HTM. On the basis of the above results, we find that the loss in the charge separation efficiency originates from fast photoexcited carrier recombination with a lifetime of 4 ps, and the loss in charge collection efficiency was due to the charge recombination occurring at the TiO₂/P3HT interface, thus leading to lower IPCE values. Also, the low V_{oc} and FF were found to result from the large Urbach energy and the recombination occurring at the TiO₂/P3HT interface. These findings indicate that the photovoltaic performance of Sn/Pb cocktail perovskite solar cells can be further improved by reducing the defects in the material and the recombination occurring at the TiO₂/HTM interface through proper interfacial engineering.

Author details

Shen Qing^{1*}, Ogomi Yuhei¹, Toyoda Taro¹, Yoshino Kenji³ and Hayase Shuzi^{2*}

*Address all correspondence to: shen@pc.uec.ac.jp; hayase@life.kyutech.ac.jp

1 Department of Engineering Science, Faculty of Informatics and Engineering, The University of Electro-Communications, Chofu, Tokyo, Japan

2 Graduate School of Life Science and Systems Engineering, Kyushu Institute of Technology, Wakamatsu, Kitakyushu, Japan

3 Department of Electrical and Electronic Engineering, Miyazaki University, Kibanadainishi, Miyazaki, Japan

This work was supported by the CREST program, Japan Science and Technology Agency (JST).

References

- [1] <http://www.nrel.gov/ncpv/>.
- [2] H. S. Jung and N.-G. Park, *Small*, 2014, 11, 10-25.
- [3] N. J. Jeon, J. H. Noh, Y. C. Kim, W. S. Yang, S. Ryu and S. I. Seok, *Nat. Mater.*, 2014, 13, 897-903.
- [4] H. Zhou, Q. Chen, G. Li, S. Luo, T.-b. Song, H.-S. Duan, Z. Hong, J. You, Y. Liu and Y. Yang, *Science*, 2014, 345, 542-546.
- [5] M. A. Green, A. Ho-Baillie and H. J. Snaith, *Nat. Photon*, 2014, 8, 506-514.
- [6] M. Z. Liu, M. B. Johnston and H. J. Snaith, *Nature*, 2013, 501, 395-398.
- [7] G. E. Eperon, V. M. Burlakov, A. Goriely and H. J. Snaith, *ACS Nano*, 2014, 8, 591-598.
- [8] J. Burschka, N. Pellet, S. J. Moon, R. Humphry-Baker, P. Gao, M. K. Nazeeruddin and M. Gratzel, *Nature*, 2013, 499, 316-319.
- [9] H. S. Kim, C. R. Lee, J. H. Im, K. B. Lee, T. Moehl, A. Marchioro, S. J. Moon, R. Humphry-Baker, J. H. Yum, J. E. Moser, M. Gratzel and N. G. Park, *Sci. Rep.*, 2012, 2, 591.
- [10] M. M. Lee, J. Teuscher, T. Miyasaka, T. N. Murakami and H. J. Snaith, *Science*, 2012, 338, 643-647.
- [11] J. H. Im, J. Chung, S. J. Kim and N. G. Park, *Nanoscale Res. Lett.*, 2012, 7, 353.
- [12] N. G. Park, *J. Phys. Chem. Lett.*, 2013, 4, 2423-2429.
- [13] G. Hodes, *Science*, 2013, 342, 317-318.
- [14] H. J. Snaith, *J. Phys. Chem. Lett.*, 2013, 4, 3623-3630.

- [15] S. Sun, T. Salim, N. Mathews, M. Duchamp, C. Boothroyd, G. Xing, T. C. Sum and Y. M. Lam, *Energy Environ. Sci.*, 2014, 7, 399-407.
- [16] S. D. Stranks, G. E. Eperon, G. Grancini, C. Menelaou, M. J. P. Alcocer, T. Leijtens, L. M. Herz, A. Petrozza and H. J. Snaith, *Science*, 2013, 342, 341-344.
- [17] G. C. Xing, N. Mathews, S. Y. Sun, S. S. Lim, Y. M. Lam, M. Gratzel, S. Mhaisalkar and T. C. Sum, *Science*, 2013, 342, 344-347.
- [18] S. De Wolf, J. Holovsky, S.-J. Moon, P. Löper, B. Niesen, M. Ledinsky, F.-J. Haug, J.-H. Yum and C. Ballif, *J. Phys. Chem. Lett.*, 2014, 5, 1035-1039.
- [19] C. C. Stoumpos, C. D. Malliakas and M. G. Kanatzidis, *Inorg. Chem.*, 2013, 52, 9019-9038.
- [20] Y. Takahashi, R. Obara, Z.-Z. Lin, Y. Takahashi, T. Naito, T. Inabe, S. Ishibashi and K. Terakura, *Dalton Trans.*, 2011, 40, 5563-5568.
- [21] F. Hao, C. C. Stoumpos, D. H. Cao, R. P. H. Chang and M. G. Kanatzidis, *Nat. Photon.*, 2014, 8, 489-494.
- [22] N. K. Noel, S. D. Stranks, A. Abate, C. Wehrenfennig, S. Guarnera, A. Haghighirad, A. Sadhanala, G. E. Eperon, S. K. Pathak, M. B. Johnston, a. petrozza, L. Herz and H. Snaith, *Energy Environ. Sci.*, 2014, 7, 3061-3068.
- [23] Y. Ogomi, A. Morita, S. Tsukamoto, T. Saitho, N. Fujikawa, Q. Shen, T. Toyoda, K. Yoshino, S. S. Pandey, T. Ma and S. Hayase, *J. Phys. Chem. Lett.*, 2014, 5, 1004-1011.
- [24] F. Hao, C. C. Stoumpos, R. P. H. Chang and M. G. Kanatzidis, *J. Am. Chem. Soc.*, 2014, 136, 8094-8099.
- [25] Q. Shen, Y. Ogomi, J. Chang, S. Tsukamoto, K. Kukihara, O. Takuya, N. Osada, K. Yoshino, K. Katayama, T. Toyoda and S. Hayase, *Phys. Chem. Chem. Phys.*, 2014, 16, 19984-19992.
- [26] A. Rosencwaig and A. Gersho, *J. Appl. Phys.*, 1976, 47, 64-69
- [27] Q. Shen, Y. Ogomi, B.-w. Park, T. Inoue, S. S. Pandey, A. Miyamoto, S. Fujita, K. Katayama, T. Toyoda and S. Hayase, *Phys. Chem. Chem. Phys.*, 2012, 14, 4605-4613.
- [28] Q. Shen, Y. Ogomi, S. K. Das, S. S. Pandey, K. Yoshino, K. Katayama, H. Momose, T. Toyoda and S. Hayase, *Phys. Chem. Chem. Phys.*, 2013, 15, 14370-14376.
- [29] N. Maeda, H. Hata, N. Osada, Q. Shen, T. Toyoda, S. Kuwahara and K. Katayama, *Phys. Chem. Chem. Phys.*, 2013, 15, 11006-11013.
- [30] N. Osada, T. Oshima, S. Kuwahara, T. Toyoda, Q. Shen and K. Katayama, *Phys. Chem. Chem. Phys.*, 2014, 16, 5774-5778.

- [31] Q. Shen, Y. Ogomi, J. Chang, T. Toyoda, K. Fujiwara, K. Yoshino, K. Sato, K. Yamazaki, M. Akimoto, Y. Kuga, K. Katayama, and S. Hayase, *J. Mater. Chem. A*, 2015, 3, 9308-9316.
- [32] F. Deschler, M. Price, S. Pathak, L. E. Klintberg, D.-D. Jarausch, R. Higler, S. Hüttner, T. Leijtens, S. D. Stranks, H. J. Snaith, M. Atatüre, R. T. Phillips and R. H. Friend, *The Journal of Physical Chemistry Letters*, 2014, 5, 1421-1426.
- [33] T. Yoshihara, R. Katoh, A. Furube, Y. Tamaki, M. Murai, K. Hara, S. Murata, H. Arawaka and M. Tachiya, *The Journal of Physical Chemistry B*, 2004, 108, 3817-3823.
- [34] R. Plass, S. Pelet, J. Krueger, M. Grätzel and U. Bach, *The Journal of Physical Chemistry B*, 2002, 106, 7578-7580.
- [35] J. J. Prías-Barragán, L. Tirado-Mejía, H. Ariza-Calderón, L. Baños, J. J. Perez-Bueno and M. E. Rodríguez, *J. Cryst. Growth*, 2006, 286, 279-283
- [36] F. Urbach, *Phys. Rev.*, 1953, 92, 1324.
- [37] K. T. H., *Phys. Rev.*, 1966, 144, 582.
- [38] K. S. and N. W., *Phys. Rev. B*, 1999, 59, 12940.
- [39] Y. Ogomi, A. Morita, S. Tsukamoto, T. Saitho, Q. Shen, T. Toyoda, K. Yoshino, S. S. Pandey, T.L. Ma, and S. Hayase, *J. Phys. Chem. C*, 2014, 118, 16651-16659.
- [40] Y. Ogomi, K. Kukihara, Q. Shen, T. Toyoda, K. Yoshino, S. Pandey, H. Momose, and S. Hayase, *Chemphyschem*, 2014.

